RSC Advances

ROYAL SOCIETY OF CHEMISTRY

www.rsc.org/advances

Determination of Adsorption Mechanism of Polycarboxylate-ether Based Superplasticizers Using Crystallization, Thermal and Mass Spectrometry Methods

Guoxing Sun[a*], Ling Wang[b], Lu-Tao Weng[c,d], Jinrui Zhang[a], Zongjin Li[a*] and Guangming Chen[e]

[a]Department of Civil and Environmental Engineering
The Hong Kong University of Science and Technology
Clear Water Bay
Hong Kong, P.R. China

[b]China Building Materials Academy
Beijing 100024, P.R. China

[c]Materials Characterization and Preparation Facility
[d]Department of Chemical and Biomolecular Engineering
The Hong Kong University of Science and Technology
Clear Water Bay
Hong Kong, P.R. China

[e]Beijing National Laboratory for Molecular Sciences (BNLMS)
Institute of Chemistry, Chinese Academy of Sciences
Beijing 100190, P.R. China

*Corresponding author. Tel.: +852-6409-1003; Fax: +852-2358-1534;
E-mail address: kesun@ust.hk.

Abstract

In this study, a series of suspensions were fabricated by dispersing calcium carbonate ($CaCO_3$), cement and silica fume into a polycarboxylate-ether plasticizer (PCE)/water solution. The PCE used was a comb-like copolymer containing a sodium polymethacrylate (PMA) backbone partially esterified with polyethyleneglycol (PEG) side chains. Sedimentation and optical microscopy tests indicated that both $CaCO_3$ and cement could form homogeneous suspensions. The crystallization behavior of the PEG side chains revealed that PEG had stronger interactions with $CaCO_3$ than with cement and silica fume particles, which were further confirmed by differential scanning calorimetry (DSC) and thermogravimetric analysis (TGA). A detailed time-of-flight secondary ion mass spectrometry (ToF-SIMS) examination suggested that PEG were mainly located on the surfaces of the $CaCO_3$, and the PMA backbones were mainly located on the surfaces of the cement and silica fume, respectively. The different interactions between copolymer and inorganic particles were associated with their interfacial tensions and had remarkable influence on the paste fluidity.

Keywords: Superplasticizer; Crystallization; Calcium carbonate; Time-of-flight secondary ion mass spectrometry; Surface tension.

Introduction

In the past three decades, polycarboxylate-ether based superplasticizers (PCEs) have attracted considerable attention due to their excellent water-reducing ability, which makes them an ideal candidate of water reducer in the manufacturing of high-performance concrete.[1, 2] A typical PCE structure is a comb-like copolymer made of a sodium polymethacrylate (PMA) backbone partially esterified with polyethyleneglycol (PEG) chains.[3] It has been proved that the increased fluidity of cement paste provided by PCE is due to the adsorption of PCE on cement particles,[4] which impose a strong static electrical field to enforce the cement particles separate.[5, 6] Furthermore, the dispersion of cement particles is amplified by the steric repulsion and hydrophilic imparting effect of the PEG side chains.[4, 7]

Calcium carbonate ($CaCO_3$) and silica fume are two important cementitious minerals in concrete.[2, 8-10] The addition of these two minerals greatly influences the fluidity of cement pastes. The interaction between the polymer and inorganic surfaces is important for paste fluidity. However, to the best of our knowledge, the interaction between PCE and inorganic binders such as $CaCO_3$ and silica fume has not been reported before. Normally, in polymer/inorganic composite systems, the interfacial force is weak[11, 12] unless chemical bonds form at the interface.[13-15] As for the adsorption of PCE on the inorganic surface, the exact adsorption mechanism is not clear. Since PCE is a copolymer with a PMA backbone and PEG side chain, the different charge and surface tensions of these two

components might contribute to the adsorption mechanism.

Although various techniques, such as rheology, atomic force microscopy (AFM), and ζ-potential, have been used to characterize the effect of PCE on cement suspensions,[16, 17] the crystallization behavior of PCE has seldom been emphasized in the investigation of adsorption mechanism. We note that in the PCE molecular structure, the PMA backbone is non-crystallizable due to the steric effect of its side groups, but PEG is a typical semi-crystalline polymer.[18] During either melt- or solvent-induced crystallization processes, PEG can develop a spherulitic morphology which can be clearly observed with a polarized optical transmission microscopy (POM).[19] Under a heterogeneous nucleation condition, the number and size of the spherulites are greatly influenced by the contacted substrate. Therefore, we can identify the interaction between PCE and inorganic surfaces from the crystallization morphology of the side chains. Moreover, thermal properties of semi-crystallized PCE such as its endothermic enthalpy and thermal stability during heating process can also be used to reflect its interaction with inorganic surfaces, because the strong interaction between polymer and inorganic surfaces can restrict the mobility of polymer chains and thus influence the crystallinity and degradation temperature.

When PCE is adsorbed on different inorganic surfaces and form a monolayer, the surface concentration of PMA backbone and PEG side chain is controlled by the different adsorption groups. Thus a detailed surface analysis can be employed to find out which group of PCE is adsorbed on the relevant inorganic surface. Besides electrostatic attraction, interfacial effect plays an important role during the adsorption

of different groups. Normally, substrate tends to adsorb group that has smaller interfacial tension.

In this study, we investigated the adsorption mechanism of PCE on the surfaces of $CaCO_3$, cement, and silica fume. First, the dispersibility and stabilization of inorganic particles in PCE solutions were characterized by sedimentation and optical microscopy (OM) tests. Then, the crystallization behavior of PCE, and detailed thermal and surface properties of PCE/inorganic composites were studied using polarized optical microscopy (POM), differential scanning calorimetry (DSC), thermogravimetric analysis (TGA), and time-of-flight secondary ion mass spectrometry (ToF-SIMS). Finally, the surface and interfacial tensions of polymer and inorganic particles were examined by contact angle measurement.

Materials and methods

Materials

The PCE/water solution with a concentration of 21.5 wt% was produced by Grace Concrete Admixture Products. Calcium Carbonate Lime Stone Powder ($CaCO_3$) was obtained from Jiangxi Guangyuan Chemical Co., Ltd. The particle sizes were 325, 600, 800 and 1250 meshes, and named as C325, C600, C800, and C1250, respectively. The average particle sizes of these four $CaCO_3$ samples were measured to be around 18, 12, 8, and 5μm, respectively, using an OMEC LC908 laser particle size analyzer. Cement that satisfies the requirements of BS EN197-1:2000 (a European standard that was adopted as a British Standard) for CEM I Portland cement of strength class 52.5

N (roughly equivalent to the requirements of ASTM C150 for Type I Portland cement) is used in this study. Silica fume particles were obtained from Elkem ASA.

Methods

Inorganic particles ($CaCO_3$, cement, and silica fume) were dispersed in PCE/water 21.5 wt% solution, respectively. The weight ratio of the inorganic particles in the solution was 4 %. The mixtures were magnetically stirred for 20 minutes then ultrasonicated for 10 minutes. Some of the suspensions were dropped onto a glass slide for OM characterization first, and then dried in a vacuum oven at room temperature for 3 days for POM characterization.

The remaining suspensions were dried in a dish in a vacuum oven at room temperature for 3 days to evaporate the solvent, then the dried paste was ground into powder and used for DSC and TGA characterizations, both with a heating rate of 10^oC/minute, in a nitrogen atmosphere. To prepare the specimens for ToF-SIMS examination, $CaCO_3$, cement, and silica fume were pressed into flat plates at 100MPa. Then the PCE/water 21.5 wt% solution was spin-coated onto the plates at a spin rate of 3000 rpm. The contact angle measurements were performed at room temperature with a G10 contact angle analyzer (Krüss GmbH Co., Germany) equipped with a video capture module.

Results and Discussion

Dispersibility and stabilization of inorganic particles in PCE solutions

The photographs of the vials of the suspensions are shown in Fig. 1. Both $CaCO_3$ and cement achieved uniform dispersion in PCE solution, though some solute still precipitated automatically at the bottom, as shown in Figs. 1a to e. Uniform and stable white dispersions were clearly visible in $CaCO_3$ dispersed in PCE solution. Further careful observations revealed that the color became darker with the decrease of $CaCO_3$ meshes (c.f. Figs. 1a to d). Moreover, in cement suspension, the color turned darker from the top to the bottom (c.f. Fig. 1e). Precipitations at the bottom together with the upper clear solution phase can be observed in Fig.1f, indicating that PCE solution is not a good dispersing medium for silica fume. The silica fume precipitation layer was at the highest height. This shows that the interaction between PCE and silica fume was the poorest in the investigation.

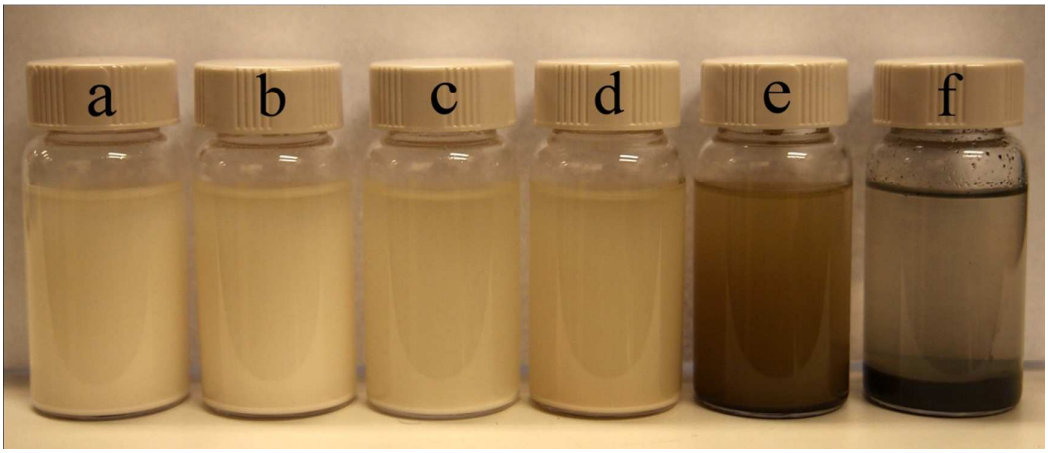

Fig. 1. Photograph of vials of $CaCO_3$, cement, and silica fume dispersed in PCE/water 21.5 wt% solution with the inorganic particle weight ratio 4 wt%. (a) C1250, (b) C800, (c) C600, (d) C325, (e) cement, and (f) silica fume, taken after magnetic stirring, ultrasonication and subsequent standing for 48 hours.

169

170 Figure 2 shows optical transmission micrographs of the dried film samples of
171 the above $CaCO_3$, cement, and silica fume dispersions. Figs. 2a to e are for $CaCO_3$
172 and cement no obvious large agglomerates, but clear individual particles can be
173 observed. The particle sizes of $CaCO_3$ with different meshes observed from the
174 optical images are consistent with the previous laser particle size analyzer result. This
175 demonstrates that the good dispersibility of $CaCO_3$ in PCE solution is not much
176 influenced by particle sizes. Normally, the particle sizes of $CaCO_3$ influence only the
177 amount of adsorbed PCE. Thus, in the following study, we focus only on the $CaCO_3$
178 of 1250 mesh. A high degree of silica fume aggregation is observed, and large
179 agglomerates with an average size of 100 μm dominate, as shown in Fig.2f. Note that
180 in the drying process of the suspensions, it is possible that the debundled inorganic
181 particles reaggregated into agglomerates due to the large surface tension. No large
182 agglomerates can be observed in Figs. 2a-e. This provides further evidence that PCE
183 solution significantly improves the dispersion and the stability of $CaCO_3$ and cement,
184 leading to the absence of large agglomerates. This is consistent with the above
185 sedimentation experimental results, and similar deduction can be found in our
186 previous work.[20]

187

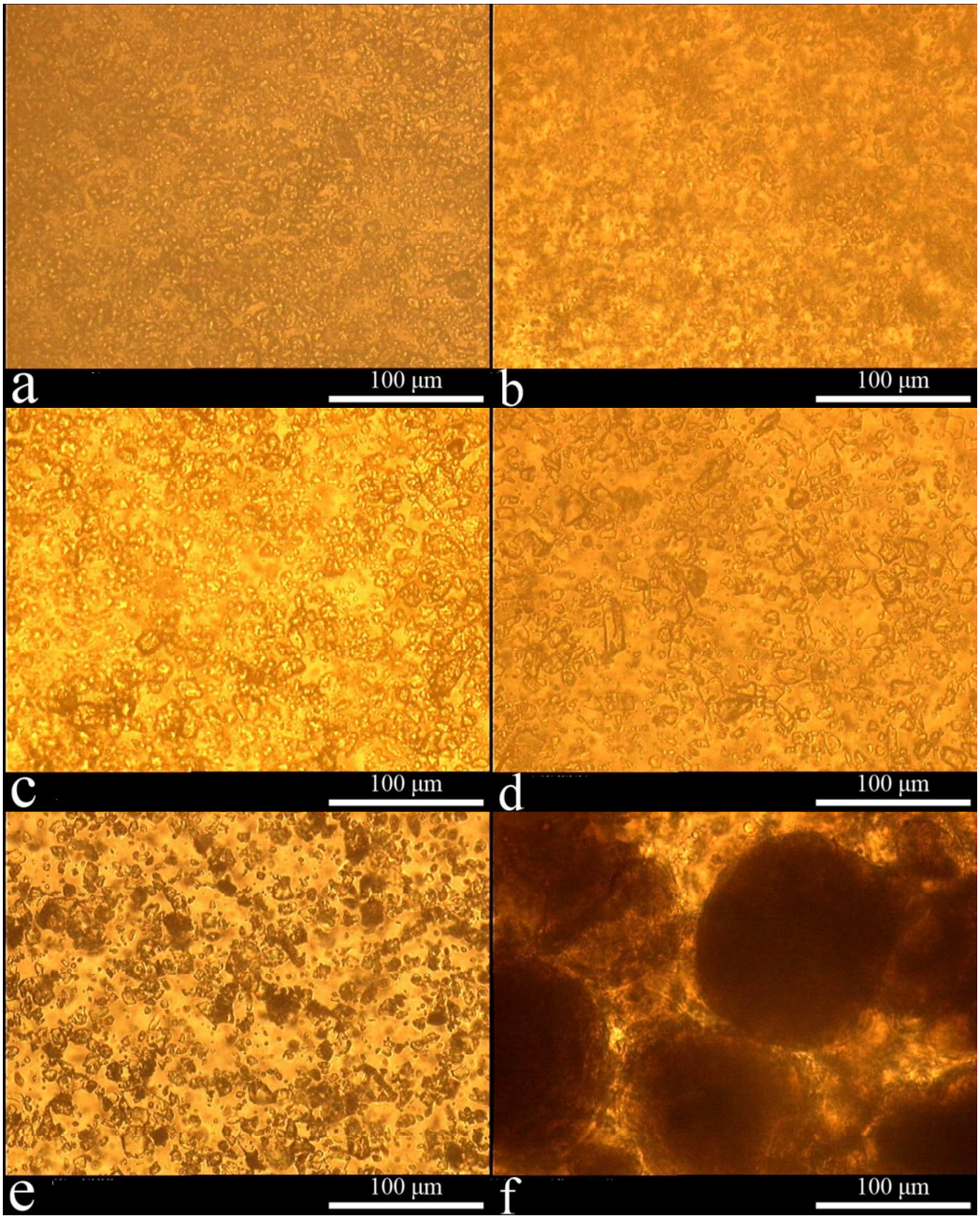

Fig. 2. Optical transmission micrographs of suspensions of $CaCO_3$, cement, and silica fume dispersed in PCE/water 21.5 wt% solution with the inorganic particle weight ratio 4 wt%. (a) C1250, (b) C800, (c) C600, (d) C325, (e) cement, and (f) silica fume. Before drying, the dispersions were magnetically stirred, subjected to ultrasonication and left standing for 48 hours.

194

195 **Crystallization morphology of PCE side chains**

196 Before demonstrating how PCE molecules interact with the inorganic particles,
197 the molecular structure of PCE is described below in detail. The PCE structure used is
198 a comb-like copolymer made of a sodium polymethacrylate (PMA) backbone partially
199 esterified with polyethyleneglycol (PEG). The chemical structure of the PCE
200 molecule is shown as below:[16]

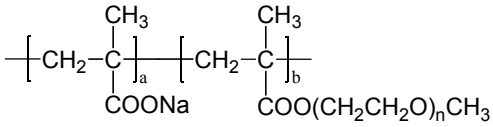

201

202

203 It is well known that PMA is non-crystallizable due to the steric effect of its
204 side groups, while PEG is a typical semi-crystalline polymer.[18] During either melt or a
205 solvent-induced crystallization process, PEG develops a spherulitic morphology
206 which can be clearly observed using a polarized optical transmission microscopy
207 (POM).[19] As shown in Fig.3a, when PCE solution is dried on a glass slide at room
208 temperature and forms a polymer film around 50 μm thick, clear spherulites with
209 diameters of around 400 μm can be observed under POM. Normally, spherulite
210 development is depending on how it is nucleated. A common progression is that a
211 spherulite begins with a fibre and evolves through sheaf-like embryos before attaining
212 a spherical envelope. Adjacent growing spherulites impinge on each other, forming
213 polygonal shapes, exactly like the single-crystalline grains of a metal.[21, 22] When the
214 solvent-induced spherulites in the film were heated to 80 ^{o}C, 20 ^{o}C higher than the

melting temperature of pure PEG,[19] the spherulites were completely melted and the window under POM turned dark. After that, the same film was cooled down to 30 °C, the amorphous PEG chains started to form crystals, and the spherulites appeared again (c.f. Fig. 3b to d). However, the melt-crystallized spherulites did not grow from the center similar to the common case mentioned above. Instead, bright crystallized parts appeared randomly in the spherulite region of Fig.3a (c.f. Fig. 3b to d). Tsitsilianis et.al. had proved that in comb-like copolymers, the crystallizable part could be phase-separated with the non-crystallizable part during the crystallization process.[23] When PCE was dried from solution, PEG crystallized and was phase-separated from PMA. At this state, PMA was in a solution state, and did not disturb the formation of PEG spherulites (c.f. Fig. 3a). However, when the PEG spherulites were melted and cooled down, PMA was in a solid state since its glass transition temperature was 130 °C.[18] So, PEG crystallized in a restricted environment due to the indurated PMA, and only formed tiny crystals in the previous spherulite region. This demonstrated how PEG crystals randomly formed in the spherulite region of Fig.3a (c.f. Fig. 3b to d).

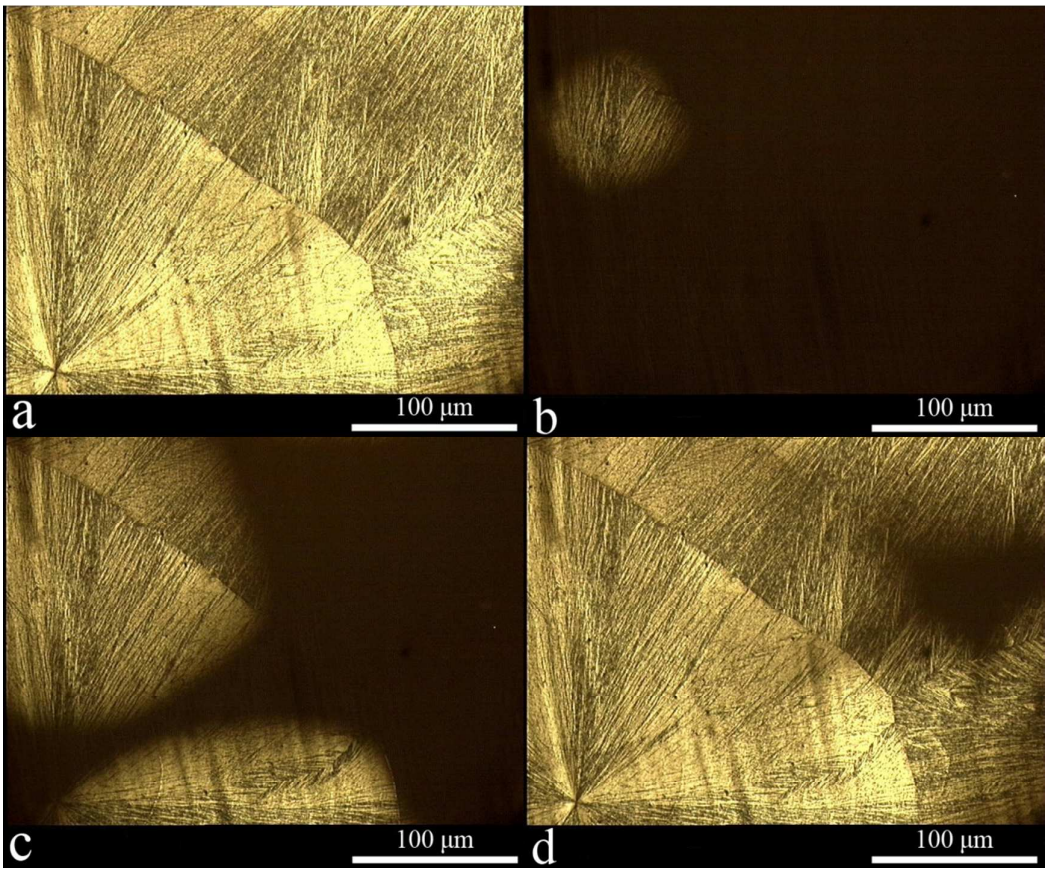

Fig. 3. Polarized optical transmission micrographs of a dried film of PCE/water 21.5 wt% solution (a) Initial sample dried from solution, (b) heated to 80 ^{o}C then cooled down to 30 ^{o}C and kept for 7 minutes, (c) kept for another 6 minutes after (b), and (d) kept for another 8 minutes after (c).

After the above detailed discussion of the crystallization behavior of PCE, the interaction between PCE and $CaCO_3$, cement, or silica fume can be examined. It is obvious that it would be more desirable if the interaction could be studied in solution. Unfortunately very few analytical techniques are available to study the interaction in solution samples. Therefore, we carried out the analysis on the dried samples and expected that the interaction can indirectly be obtained from these samples. The

heterogeneous nucleation during the formation of PEG spherulites is employed in the below discussion. In Fig. 3, a PCE solution with no impurities was dropped onto a clean glass slide. During the solvent-induced crystallization process, the heterogeneous nucleation effect was weak, and PEG formed spherulites had a diameter of 400 μm. When the suspensions of PCE and $CaCO_3$, cement, or silica fume were dried and spherulites were formed, because of the heterogeneous nucleation effect of these inorganic particles, the number of spherulites increased and the size of the spherulites decreased as compared to those in Fig. 3 (c.f. Fig. 4a, c and e). Among the three PCE/inorganic particle systems, $CaCO_3$ had the strongest heterogeneous nucleation effect due to the large number and small size of PEG spherulites from PCE/$CaCO_3$ suspension (c.f. Fig. 4a). In contrast, fewer large spherulites were generated during the drying process of the PCE/cement and PCE/silica fume suspensions (c.f. Fig. 4c and e). The interaction of PEG side chains with cement or silica fume was weaker than that of $CaCO_3$. The POM images in Fig. 4b, d and f were obtained by heating the samples in Fig. 4a, c and e to 80^{o}C then cooling down to 30^{o}C and keeping for 60 min. As can be seen from the figures, during the melt-crystallization process, spherulites became darker and indistinct, indicating that the crystallinity of PEG decreased. It was proved that the mobility of polymer chains was restricted within 30 nm to the solid substrate.[24] During the melt-crystallization process, both the indurated PMA and inorganic particles restricted the PEG chain mobility and decreased its crystallinity. The spherulites formed in the PCE/$CaCO_3$ system were the darkest (c.f. Fig.4b), indicating that the crystallinity of PEG was the

lowest, so the contact of PEG to $CaCO_3$ was stronger than that of cement and silica fume.

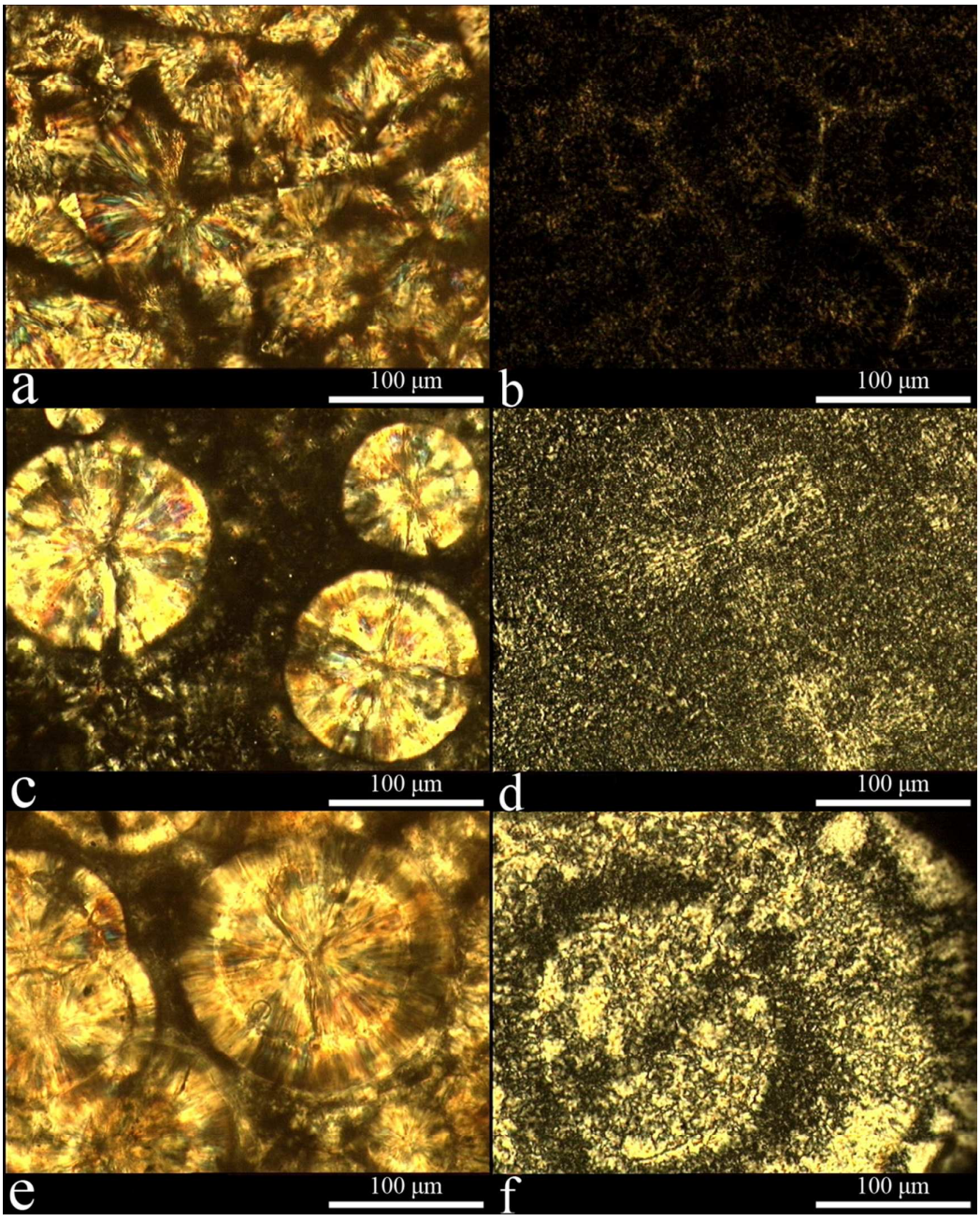

Fig. 4. Polarized optical transmission micrographs of dried samples of $CaCO_3$, cement, and silica fume dispersed in PCE/water 21.5 wt% solution with the inorganic particle weight ratio 4 wt%. (a) $CaCO_3$, (c) cement, and (e) silica fume. (b), (d) and (f) are the

samples in (a), (c) and (e) heated to 80^{o}C then cooled down to 30^{o}C and kept for 60 minutes, respectively.

Thermal analysis of PCE/inorganic composites

To confirm the above results inferred from the crystallization morphology of PEG, a DSC test was employed to study the heating and cooling process of PCE and PCE/inorganic composites dried from the solution. As shown in Fig.5a, during the heating process, an endothermic peak around 50^{o}C can be observed in both PCE and the composites. This peak represents the melting of PEG crystals that formed during the drying process. In Table 1 we can see that the endothermic enthalpy of PCE/$CaCO_3$ is 89.1 J/g, which is much lower than the others. This demonstrates that the crystallinity of PEG is lower than the others when it interacts with $CaCO_3$ during the solvent-induced crystallization process. Fig.5b shows the cooling process of PCE and the composites. PCE generates an exothermic peak at 19.7 ^{o}C, which is about 10 ^{o}C lower than that of the other three composites. The reason is the heterogeneous nucleation of pure PCE is weak, so it is difficult for PCE to crystallize at high temperature. However, with the interaction of $CaCO_3$, melt-crystallization can occur even at a temperature of 29.8 ^{o}C, which is also higher than the exothermic peak temperatures of the composites containing cement and silica fume. This provides further evidence that $CaCO_3$ has the strongest interaction with PEG side chains when it is dispersed into a PCE solution. The strong interaction between PEG and $CaCO_3$ also caused the lowest crystallinity of PEG during the melt-crystallization process, as demonstrated by the lowest exothermic enthalpy of 68.7 J/g (c.f. Table 1).

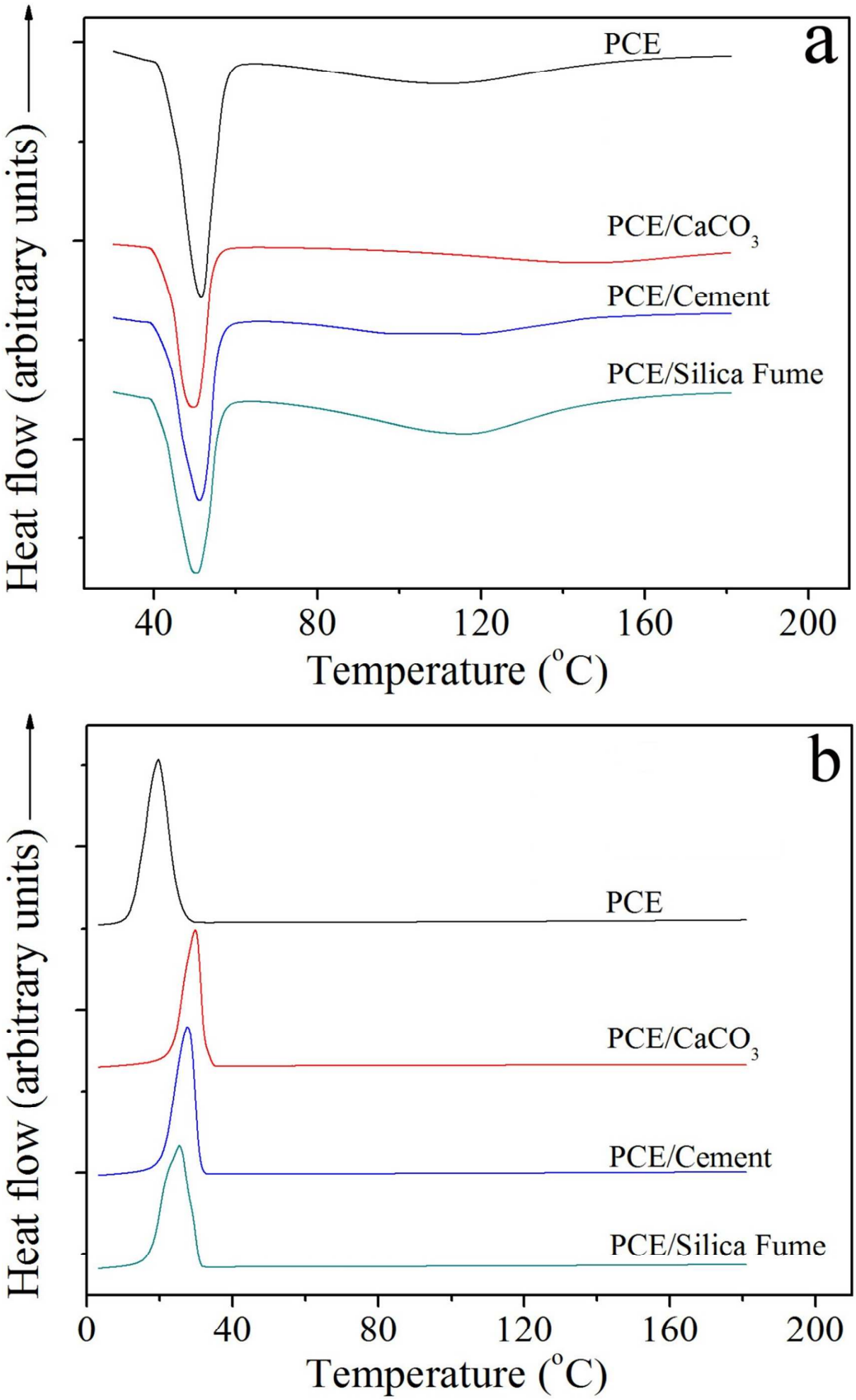

293

Fig. 5. DSC thermograms of dried samples of PCE and $CaCO_3$, cement, and silica fume dispersed in PCE/water 21.5 wt% solution with the inorganic particle weight ratio 4 wt%. (a) Heating process, and (b) cooling process, with a rate of 10 ^oC/minute, under nitrogen.

Table1. Endothermic and exothermic peak temperatures (T_p) and associated enthalpies (ΔH) of dried samples of PCE and inorganic particles dispersed in PCE/water 21.5wt% solution with the inorganic particle weight ratio 4 wt%, as obtained from the thermograms of DSC and their derivative.

Specimen	Endothermic peak temperatures and associated enthalpies		Exothermic peak temperatures and associated enthalpies	
	T_p (^oC)	ΔH (J/g)	T_p (^oC)	ΔH (J/g)
PCE	51.5	108.0	19.7	83.7
PCE/$CaCO_3$	49.6	89.1	29.8	68.7
PCE/cement	51.1	105.9	27.8	82.2
PCE/silica fume	50.1	101.3	25.5	77.8

The difference of the interaction between PCE and different inorganic particle can also be seen from TGA tests. As shown in Fig. 6, the onset decomposition temperature (T_{onset}) and the temperature at the maximum degradation rate (T_{max}, determined from the derivative of TGA curve) of PCE/$CaCO_3$ is 364 and 390^oC,

respectively. In contrast, both PCE/cement and PCE/silica fume under the same processing condition shows much lower T_{onset} (355^{o}C) and T_{max} (376^{o}C). The increases of the T_{onset} and T_{max} are 9 and 14 ^{o}C, respectively. The strong interaction between PCE and $CaCO_3$ may prevent polymer chains from debundling and degradation, and significantly improve thermal stability.

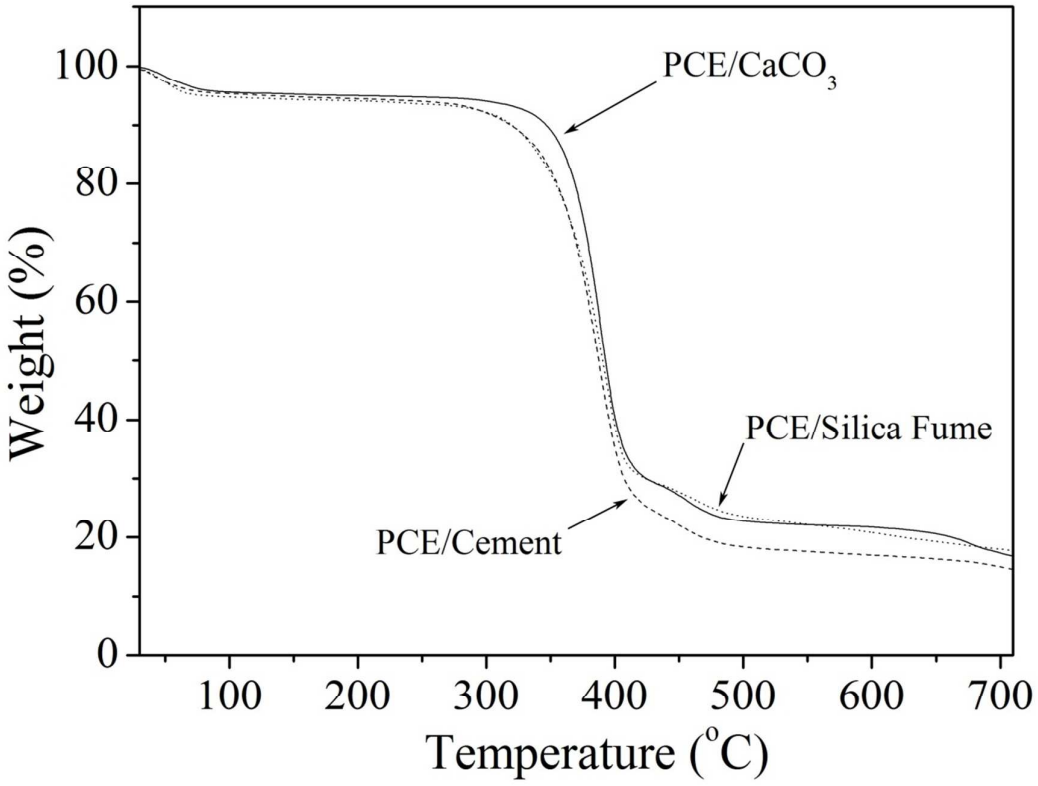

Fig. 6. TGA heating diagrams of dried samples of $CaCO_3$, cement, and silica fume dispersed in PCE/water 21.5 wt% solution with the inorganic particle weight ratio 4 wt%, with a heating rate of 10 ^{o}C/minute, under nitrogen.

Interfacial effect between PCE and inorganic surfaces

The strong interaction between $CaCO_3$ and PEG side chains indicates a possibility that most PEG side chains adsorbed onto the $CaCO_3$ surface instead of

PMA backbone when $CaCO_3$ was mixed with PCE solution. To investigate the distributions of PEG side chains and PMA backbone on the surfaces of inorganic particles, ToF-SIMS was used to determine the surface chemical composition of the PCE-coated inorganic plates. Positive ion $C_3H_7O^+$ was chosen to represent PEG side chains while $C_4H_7O_2^+$ was chosen to represent PMA backbone. The peak area ratio of $C_3H_7O^+$ to $C_4H_7O_2^+$ was used to represent the concentration ratio of PEG to PMA. The ToF-SIMS results of the specimens of PCE/water 21.5 wt% solution spin-coated on the surfaces of $CaCO_3$, cement, and silica fume plates showed that the PEG-to-PMA ratio on the surface of the $CaCO_3$ plate was much lower than that on the surface of the pure PCE, cement, and silica fume plates (c.f., Fig. 7). Therefore, from the surface chemical composition of these PCE-coated inorganic plates, we can conclude that most PEG side chains adsorbed onto the $CaCO_3$ surface, while the PMA backbone mainly adsorbed onto the surface of cement and silica fume. The higher PEG-to-PMA ratio on cement surface than that of the neat PCE surface partially supports the argument that in cement paste, PCE adsorbs onto positively charged surface sites of the cement particles with their anionic trunk polymer chain. The part of the cement particles carrying a cationic charge is neutralized by the PCE.[7]

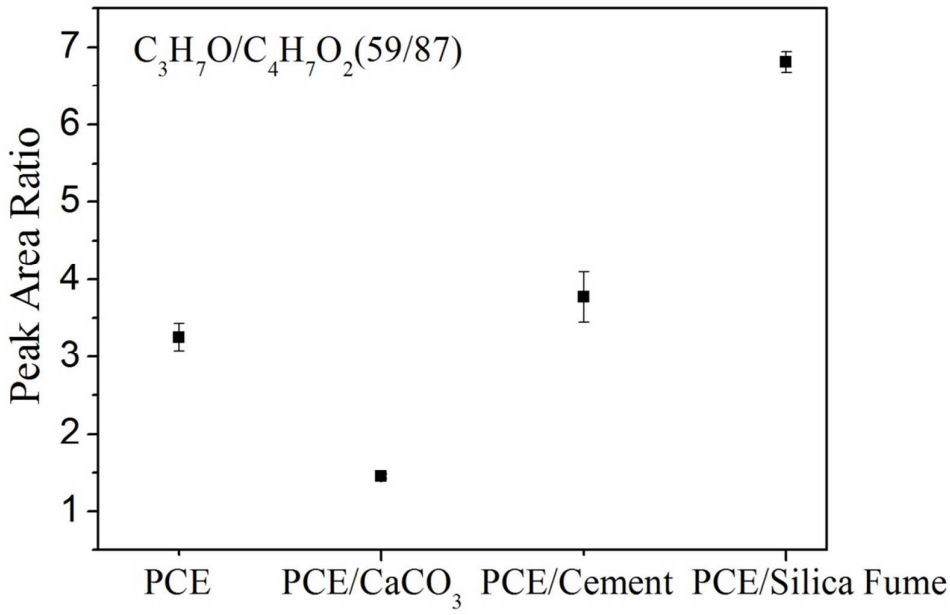

Fig. 7. Ratios of the peak intensity of the positive ion C_3H_7O (59) representing PEG to the peak intensity of the positive ion $C_4H_7O_2$ (87) representing PMA obtained from a spin-coated film of PCE/water 21.5 wt% solution on $CaCO_3$, cement, and silica fume plates at a spin rate of 3000 rpm.

To elucidate the mechanism of the adsorption of PCE on the surfaces of $CaCO_3$, cement, and silica fume, the interfacial effect between PCE or PMA and inorganic particles was investigated in detail. In order to get the interfacial tensions between polymer and inorganic substrates, the relevant surface tensions were measured using a contact angle method. For PEG and PMA, the contact angle θ can be easily obtained by dropping the test liquids onto the as-formed polymer films. However, since $CaCO_3$, cement and silica fume are all powder samples, the relevant contact angle θ has to be calculated using the Washburn equation (1):[25]

$$x^2 = \frac{Rt}{2\eta}\gamma_l \cdot \cos\theta \quad (1)$$

where, x is the penetrating distance of the liquid at the time t through the powdered substrate, η is the viscosity of the liquid, R is the effective pore size, and γ_l is the surface tension of the liquid. In Table 2, viscosities and surface tensions including dispersive and polar components of the used test liquids are listed.

Table 2. Viscosities and surface tensions including dispersive and polar components of the test liquids at 25°C used in the contact angle method.[26]

Test liquid	Viscosity (η)	Surface tension (mJ/m^2)		
		Dispersive (γ_l^d)	Polar (γ_l^p)	Total (γ_l)
n-Hexane	0.307	18.43	0	18.43
Water	0.8937	21.8	51.0	72.8
Ethyl Glycol	20.93	30.9	16.8	47.7

The surface tensions of polymer and inorganic powder are calculated using the geometric-mean equation (2):[27]

$$\gamma_l(1 + \cos\theta) = 2\left[\left(\gamma_l^d\gamma_s^d\right)^{1/2} + \left(\gamma_l^p\gamma_s^p\right)^{1/2}\right], \quad (2)$$

where θ is the contact angle obtained as mentioned above, γ_l is the surface tension of the liquid, γ_l^d and γ_l^p are the dispersive and polar components of the surface tension of the liquid, and γ_s^d and γ_s^p are the dispersive and polar components of the surface tension of the solid, respectively. The equation has been described in detail in our previous work.[22, 28] The values are shown in Table 3.

Table 3. Surface tensions of PEG, PMA, $CaCO_3$, cement and silica fume measured using the contact angle method and calculated using Eq. 2.

Material	Surface tension (mJ/m^2)		
	Dispersive (γ_s^d)	Polar(γ_s^p)	Total(γ_s)
PEG	8.2±0.5	32.1±1.2	40.3±0.9
PMA	14.2±0.3	32.9±0.5	47.1±0.7
$CaCO_3$	2.9±0.3	56.8±1.1	59.7±1.0
Cement	502.3±3.2	25.9±1.5	528.2±2.6
Silica Fume	17.7±0.6	26.2±1.8	43.9±1.3

The interfacial tension between the polymer and inorganic substrate, $\gamma_{1,2}$, is calculated using the geometric-mean equation (3):[27]

$$\gamma_{1,2} = \gamma_1 + \gamma_2 - 2\sqrt{\gamma_1^d \gamma_2^d} - 2\sqrt{\gamma_1^p \gamma_2^p}, \quad (3)$$

where γ_1 is the surface tension of medium 1, and γ_1^d and γ_1^p are the dispersive and polar components of the surface tension of medium 1, respectively. The interfacial tensions between polymer and inorganic substrate are calculated using Eq. 3 and the results are shown in Table 4. These results indicate that $CaCO_3$ tends to adsorb PEG instead of PMA, because the interfacial tension between $CaCO_3$ and PEG is lower than that between $CaCO_3$ and PMA. In contrast, cement and silica fume adsorb PMA more easily due to their lower interfacial tension than that of PEG. This conclusion is in agreement with the above ToF-SIMS results.

386 It is clear from the above crystallization and thermal study that the interaction of
387 PCE with $CaCO_3$ is stronger than those with cement and silica fume. This is in
388 agreement with the dispersibility measurements of these inorganic particles in PCE
389 solution. Furthermore, based on the findings obtained from the ToF-SIMS and
390 interfacial energy measurements, the detailed adsorption mechanism of PCE on the
391 surfaces of inorganic particles can be deduced. The backbone and side chain of PCE
392 adsorb on the surfaces of cement and $CaCO_3$ respectively, due to the different
393 interfacial tension. This finding would be very useful for the selection criterion of
394 inorganic fillers and to identify their compatibility with superplasticizers. Also if the
395 adsorption behavior of the superplasticizer on the surfaces of selected inorganic fillers
396 is determined, their influence on the fluidity can be predicted. For example, based on
397 the adsorption behavior of PCE on the surfaces of cement and $CaCO_3$, the addition of
398 $CaCO_3$ to cement will not reduce the fluidity of cement paste as demonstrated by the
399 fluidity test described in the following part.
400

401 **Table 4.** Interfacial tensions between PEG, PMA and $CaCO_3$, cement and silica
402 fume, calculated using Eq. 3.

Interface tension (mJ/m^2)	Polymers	
	PEG	PMA
$CaCO_3$	4.8±0.3	7.5±0.8
Cement	382.5±3.7	348.0±5.2
Silica Fume	2.10±0.1	0.57±0.2

403

404 **Fluidity test**

405 The performance of the different adsorption of PCE on the surfaces of
406 $CaCO_3$ and cement can be seen from the fluidity of the cement/$CaCO_3$ paste. The
407 fluidity was determined by the spread diameter of cement paste with the presence and
408 absence of $CaCO_3$ after slump cone was lifted. As shown in Fig. 8, the spread
409 diameter of cement paste apparently decreases with time, indicating the fluidity
410 decreases during the hydration process. With the addition of 20 wt% and 30 wt%
411 $CaCO_3$, represented by cement/$CaCO_3$ ratio (80/20) and (70/30), the fluidity decrease
412 with time is obviously reduced. The dosage of PCE/water solution (21.5 wt%) in
413 cement, cement/$CaCO_3$ (80/20) and (70/30) was 0.40 wt%, which is decided by
414 controlling the initial spread diameter to be 260±5 mm. This demonstrated that $CaCO_3$
415 could improve the fluidity of cement paste. Since $CaCO_3$ mainly adsorbs the PEG side
416 chains, while cement mainly adsorbs the PMA backbone, the addition of $CaCO_3$ did
417 not influence the interaction between cement and PCE. Further, the steric repulsion of
418 PEG side chains was amplified due to the adsorption on $CaCO_3$ particles, resulting in
419 an increase of dispersion of cement particles. Therefore, the fluidity of cement/$CaCO_3$
420 had been improved dramatically during the cement hydration process.

421

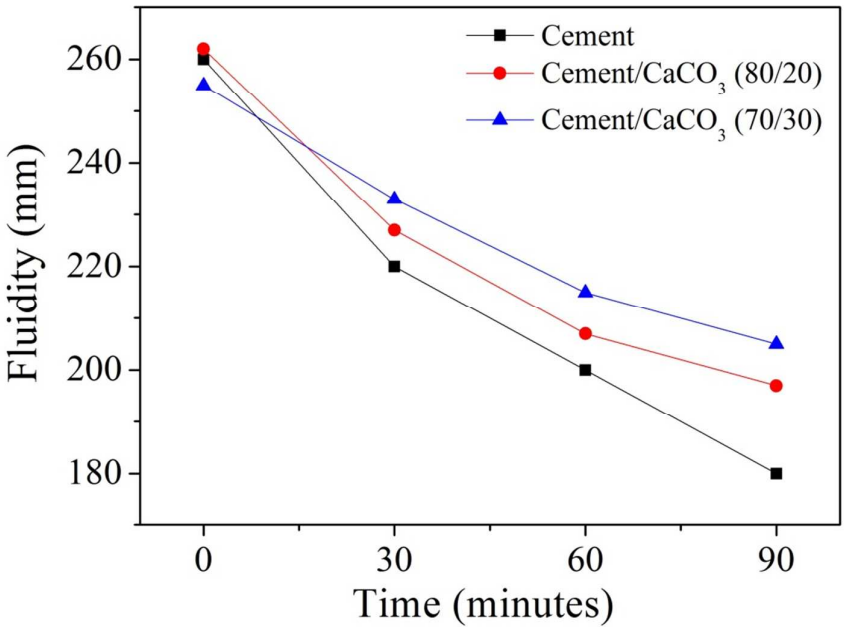

Fig. 8. Fluidity of cement paste (W/C=0.3) according to time with the addition of $CaCO_3$.

Conclusions

The adsorption mechanisms of polycarboxylate-ether based superplasticizers on the surface of $CaCO_3$, cement, and silica fume were investigated using several methods in this study. The strong interaction between $CaCO_3$ and the PEG side chains of the superplasticizer was firstly demonstrated by the crystallization behavior of PEG. In this work, ToF-SIMS was used to prove that $CaCO_3$ mainly adsorbed PEG side chains, while cement and silica fume mainly adsorbed PMA backbone. So, $CaCO_3$ could improve the fluidity of cement paste. The adsorption mechanism was explained by interfacial effect based on the measured interfacial tensions between the superplasticizer and inorganic surfaces. This work opens new avenues to the future analysis of mechanism of superplasticizers and to the selection

criterion of inorganic fillers.

Acknowledgement

The financial support from Hong Kong Research Grants Council under the grant of 615412 is gratefully acknowledged.

Reference

1. B. H. Guan, Q. Q. Ye, J. L. Zhang, W. B. Lou and Z. B. Wu, *Cem. Concr. Res.*, 2010, 40, 253-259.
2. J. Plank, C. Schroefl, M. Gruber, M. Lesti and R. Sieber, *J. Adv. Concr. Technol.*, 2009, 7, 5-12.
3. S. Pourchet, S. Liautaud, D. Rinaldi and I. Pochard, *Cem. Concr. Res.*, 2012, 42, 431-439.
4. H. Uchikawa, S. Hanehara and D. Sawaki, *Cem. Concr. Res.*, 1997, 27, 37-50.
5. Z. Li, *Advanced concrete technology*, Wiley, Hoboken, N.J., 2011.
6. D. Hou, H. Ma, Y. Zhu and Z. Li, *Acta Mater.*, 2014, 67, 81-94.
7. J. Ruhe, M. Ballauff, M. Biesalski, P. Dziezok, F. Grohn, D. Johannsmann, N. Houbenov, N. Hugenberg, R. Konradi, S. Minko, M. Motornov, R. R. Netz, M. Schmidt, C. Seidel, M. Stamm, T. Stephan, D. Usov and H. N. Zhang, *Polyelectrolytes with Defined Molecular Architecture I*, 2004, 165, 79-150.
8. P. De Silva, L. Bucea and V. Sirivivatnanon, *Cem. Concr. Res.*, 2009, 39, 460-465.
9. T. Matschei, B. Lothenbach and F. P. Glasser, *Cem. Concr. Res.*, 2007, 37, 551-558.
10. C. Schrofl, M. Gruber and J. Plank, *Cem. Concr. Res.*, 2012, 42, 1401-1408.
11. G. X. Sun, G. M. Chen, J. Liu, J. P. Yang, J. Y. Xie, Z. P. Liu, R. Li and X. Li, *Polymer*, 2009, 50, 5787-5793.
12. G. X. Sun, G. M. Chen, Z. P. Liu and M. Chen, *Carbon*, 2010, 48, 1434-1440.
13. H. Y. Ma, Y. Tian and Z. J. Li, *J. Mater. Civ. Eng.*, 2011, 23, 1412-1421.
14. H. Ma and Z. Li, *Constr. Build. Mater.*, 2013, 47, 579-587.
15. A. Stewart, B. Schlosser and E. P. Douglas, *ACS Appl. Mater. Interfaces*, 2013, 5, 1218-1225.
16. L. Ferrari, J. Kaufmann, F. Winnefeld and J. Plank, *Cem. Concr. Res.*, 2011, 41, 1058-1066.
17. K. Yamada, *Cem. Concr. Res.*, 2011, 41, 793-798.
18. J. E. Mark and Books24x7 Inc., Oxford University Press,, Oxford ; Hong Kong, 2nd edn., 2009, pp. 1 online resource (vii, 1240 p.).
19. C. Nakafuku and M. Sakoda, *Polymer Journal*, 1993, 25, 909-917.
20. G. X. Sun, Z. P. Liu and G. M. Chen, *Nano*, 2010, 5, 103-109.
21. D. C. Bassett, in *Cambridge solid state science series*, Cambridge University Press,, Cambridge, 1981.
22. G. X. Sun, L.-T. Weng, J. M. Schultz and C. M. Chan, *Polymer*, 2014, 55, 1829-1836.
23. C. Tsitsilianis, D. Papanagopoulos and P. Lutz, *Polymer*, 1995, 36, 3745-3752.
24. Y. Wang, C. M. Chan, K. M. Ng and L. Li, *Macromolecules*, 2008, 41, 2548-2553.

25. P. M. Costanzo, W. Wu, R. F. Giese and C. J. Vanoss, *Langmuir*, 1995, 11, 1827-1830.
26. I. M. Smallwood, Arnold,, London, 1996, pp. xxi, 306 p.
27. D. K. Owens and R. C. Wendt, *J. Appl. Polym. Sci.*, 1969, 13, 1741-1747.
28. G. X. Sun and C. M. Chan, *Colloid. Polym. Sci.*, 2013, 291, 1495-1501.